

Neural-network-based spatial light-scattering instrument for hazardous airborne fiber detection

Paul Kaye, Edwin Hirst, and Zhenni Wang-Thomas

A laser light-scattering instrument has been designed to facilitate the real-time detection of potentially hazardous respirable fibers, such as asbestos, within an ambient environment. The instrument captures data relating to the spatial distribution of light scattered by individual particles in flow by use of a dedicated multielement photodiode detector array. These data are subsequently processed with an artificial neural network that has previously been trained to recognize those features or patterns within the light-scattering distribution that may be characteristic of the specific particle types being sought, such as, for example, crocidolite or chrysotile asbestos fibers. Each particle is thus classified into one of a limited set of classes based on its light-scattering properties, and from the accumulated data a particle concentration figure for each class may be produced and updated at regular intervals. Particle analysis rates in excess of $10^3/s$ within a sample volume flow rate of 1 l/min are achievable, offering the possibility of detecting fiber concentrations at the recommended maximum exposure limit of 0.1 fibers/ml within a sampling period of a few seconds. © 1997 Optical Society of America

Key words: Light scattering, fibers, asbestos, neural networks.

1. Introduction

The *in situ* detection of potentially hazardous respirable fibers has become a growing concern within industrialized countries as the health risks associated with these fibers have become more fully understood. The most commonly encountered hazardous fibers are of asbestos materials that, despite a widespread ban on their use for many years, are still present in vast quantities in public and commercial buildings and plants throughout the world. The most abundant asbestos mineral, chrysotile (or white) asbestos, is present in over 95% of these installations. The second most commonly found variety is crocidolite (or blue) asbestos, with amosite (or brown) asbestos being a third but much rarer form. Scanning electron micrographs of crocidolite and chrysotile materials are shown in Fig. 1. Crocidolite and amosite belong to the amphibole class and are characterized by the fine, straight, needlelike fibers produced when the material is fragmented. Chrysotile asbestos belongs to the serpentine class of min-

erals and is characterized by a natural curvature in the fibers it produces. All three materials produce fibers that are capable of penetrating deep into the lung and that, because of their shape, become entrapped there. Crocidolite and amosite fibers are known to be far more carcinogenic than those of chrysotile asbestos, and although the exact reasons for this are still not confirmed, the half-life of the fibers in the lung (a function of the body's ability to chemically dissolve the fibers) is believed to play a major role¹ since this may be measured in decades for amphibole fibers compared with months for chrysotile fibers.

The recent *Lancet* paper by Peto *et al.*² in which the authors discuss the continuing increase in mesothelioma mortality in Britain has highlighted once again the potential hazard of respirable asbestos fibers generated during clearance operations or routine building maintenance work. Indeed, the high rates of disease associated with asbestos inhalation resulted in the statement in 1990 by the U.S. National Institute for Occupational Safety and Health (NIOSH) that there is "no evidence for a threshold or 'safe' level of asbestos exposure".³

A. Airborne Fiber Measurement

The most commonly used method for the assessment of airborne fiber concentrations is by filter cassette sampling followed by phase contrast light microscope counting of fibers. Stringent counting rules are laid

The authors are with the Engineering Research and Development Centre, University of Hertfordshire, Hatfield, Hertfordshire AL10 9AB United Kingdom.

Received 14 January 1997; revised manuscript received 28 April 1997.

0003-6935/97/246149-08\$10.00/0

© 1997 Optical Society of America

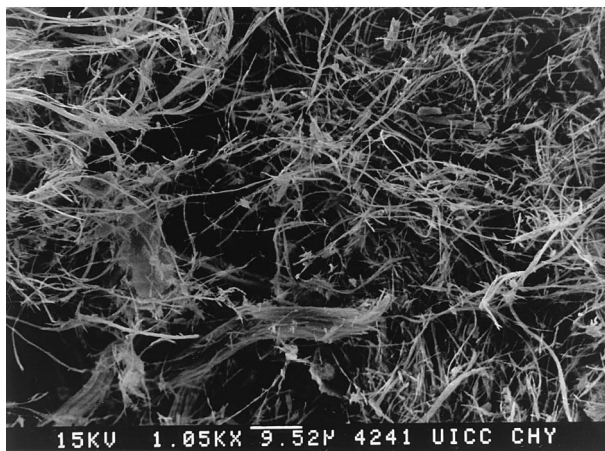
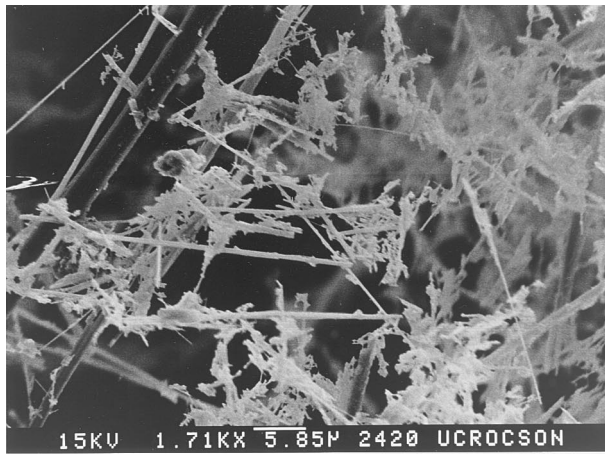


Fig. 1. Scanning electron micrographs of crocidolite asbestos (top) and chrysotile asbestos (bottom) showing the characteristic needle-like and curved fibers, respectively. Fiber diameters range from submicrometer to a few micrometers.

down in standards, such as NIOSH 7400,⁴ which detail the size and aspect ratios of particles to be counted as fibers and define how to deal with inevitable occurrences of crossed fibers, fibers attached to other particles, and fibers lying partly outside the measurement template. In the NIOSH standard, only particles greater than 5 μm in length with an aspect ratio greater than 3:1 are counted as fibers, whereas fibers with a diameter greater than 3 μm or that are attached to other particles greater than 3 μm in diameter are not counted. The counting processes are laborious and expensive to perform and, perhaps most importantly, provide results only many hours after the sampling (and possible inadvertent exposure of personnel) has occurred. Numerous attempts have therefore been made by other researchers to address methods by which real-time or *in situ* detection of airborne asbestos and other potentially hazardous fibers can be achieved.

A well-established instrument for airborne fiber

measurement is the FAM-7400 fibrous aerosol monitor (Mie, Inc., Bedford, Massachusetts) developed originally by Lilienfeld *et al.*⁵ in 1979. This instrument draws air containing the airborne particles through a laser scattering chamber that is enveloped by a quadruple electrode arrangement. When a time-varying signal is applied to the electrodes, the electric field within the scattering chamber causes conducting fibers that are present in the air to oscillate. (Asbestos fibers generally fall into this category because of their high water adsorption.) The consequent cyclic variation in light scattered by the fibers to a single light detector at the side of the chamber is used to assess fiber concentration in the air. The FAM-7400 is capable of detecting individual fibers within the scattering chamber though the geometry of its detection volume may lead to comparatively high coincidence losses of typically $\sim 15\%$ at a measured concentration of 15 fibers/ml.⁶ Its comparatively low sample throughput may also lead to prolonged sampling times. For example, counting 10 fibers at the NIOSH action limit of 0.1 fibers/ml for occupational exposure requires ~ 10 min sampling time.

More recently, Rood *et al.*⁷ have described a low-cost portable fiber monitor developed at the U.K. Health and Safety Executive Laboratories. This device is based on the differential light scattering produced by fibrous particles that are deposited electrostatically in uniform alignment onto a glass substrate. It is capable of detecting airborne asbestos fibers but is not designed to detect individual particles, relying instead on the summation of scattering signals from a multitude of deposited fibers so as to achieve a detectable signal. Rood *et al.* state that the U.K. clearance limit for asbestos in buildings of 0.01 fibers/ml can be detected after approximately 300 min sampling time.

In theory, the detailed spatial intensity distribution of light scattered by individual particles (the scattering profile) contains information relating to the particle's size, shape, and orientation with respect to the incident illumination. It is also a function of the wavelength and polarization of the incident illumination. In the research reported here we have sought to exploit characteristic features of the scattering profiles of, primarily, chrysotile and crocidolite asbestos fibers, with the aim of facilitating the rapid discrimination of each type of fiber from other particles present within an ambient environment.

B. Spatial Laser Scattering Profiles

Scattering profiles from a wide variety of particle types have been studied by the authors to verify scattering characteristics, to aid the validation of theoretical models (see, for example, Hirst *et al.*⁸), and to provide the basis for practical instruments for particle shape classification. Conventional optical scattering instruments used for particle counting and sizing normally rely on the collection of scattered light with a single discrete detector. Such instru-

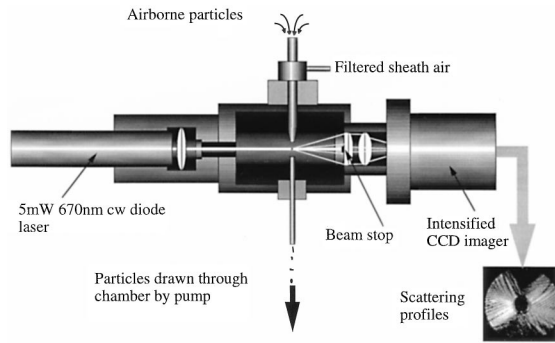


Fig. 2. Schematic diagram of the laser scattering test chamber used to collect high-resolution scattering profiles from individual particles carried in a sample airstream.

ments cannot provide information on particle shape and, indeed, normally assume that all measured particles are spherical when ascribing a size value to them. When several detectors are used, each collecting light over a different solid angle within the sphere of scattering around the particle, some shape as well as size information is obtainable, and this principle is embodied in an earlier instrument developed by the authors (Kaye *et al.*⁹).

To extract more subtle information relating to particle morphology, the spatial intensity distribution of light scattered by the particle must be recorded in more detail. The exact configuration of detectors used to record this information is inevitably a compromise between the level of detail sought and the number of detectors, and hence data processing time, that can be tolerated. To establish an optimal detector configuration (in terms of number, geometry, etc.) for the desired analysis of asbestos fiber spatial scattering, it was first necessary to record the spatial scattering profiles from these fibers and other particulates at sufficient resolution to allow detailed mod-

eling to take place. This was achieved with a laser scattering test chamber that incorporated an intensified CCD camera to record scattering profiles from particles illuminated by a 5-mW, 670-nm diode laser. This test chamber is shown schematically in Fig. 2. In brief, airborne particles are drawn through the chamber in a sample airstream that is ensheathed in a layer of filtered air. These combined laminar flows are aerodynamically focused such that the sample air column passes through the central region of an incident laser beam, the beam being linearly polarized in the plane of the diagram. This focusing also has the effect of tending to align elongated particles with their long axis parallel to the axis of flow. The light scattered at angles from 5° to 30° to the beam axis and throughout 360° of azimuth is recorded by the CCD camera as the particle traverses the beam, and this image is passed to a host computer for storage. The system is comparatively slow, recording and storing approximately two images per second.

Figure 3 shows examples of scattering profiles recorded from various particle types. The top row shows scattering profiles from a variety of background particles: those of irregular shape (most commonly encountered), droplets, and regular crystalline shape (normally rare). The second and third rows show profiles recorded from crocidolite and chrysotile asbestos fibers, respectively. The images illustrate the wide variety of scattering profiles that may be encountered from different particle morphologies as well as the preferential vertical orientation (and predominantly horizontal scattering) exhibited by the fibrous particles within the sample flow. The asbestos fiber measurements were recorded from aerosols that had been produced from dry asbestos powders with Union Internationale de la recherche Contre le Cancer reference materials. The signal dynamic range achievable by the instrument allowed capture of scattering profiles from fibers from a few

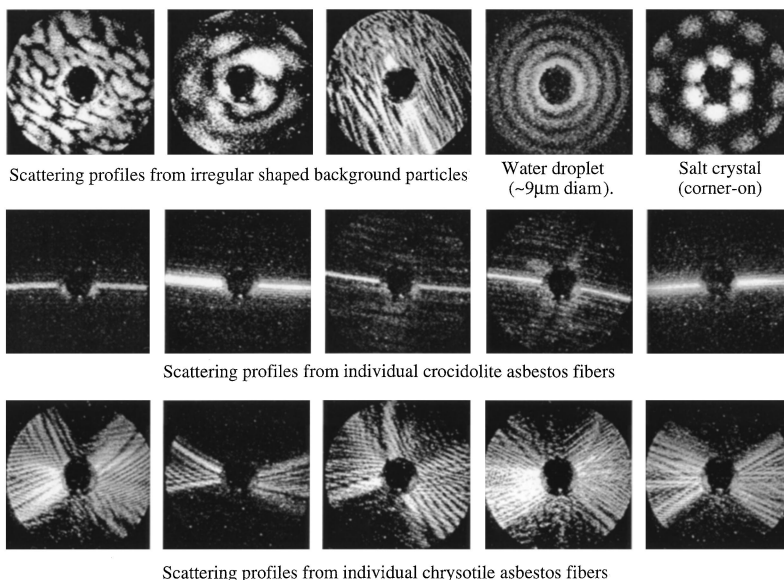


Fig. 3. Examples of scattering profiles recorded from individual airborne particles. The upper row illustrates the wide variety of profiles derived from typical background particles; the center row shows profiles from individual crocidolite asbestos fibers; and the lower row shows profiles from individual chrysotile asbestos fibers.

micrometers to $\sim 20 \mu\text{m}$ in length and from $\sim 0.25 \mu\text{m}$ and up in thickness.

As illustrated in Figure 3, the chrysotile and crocidolite fiber profiles showed some significant differences. The chrysotile fibers, being normally curved, caused the scattering profiles to assume a bow tie appearance where the scattering is still predominantly horizontal, but the differing inclinations of incremental sections of fiber length to the incident illumination cause the fine divergent structure shown. The crocidolite material, in contrast, produces straight fibers of more regular morphology that result in extremely well-defined horizontal scattering. The width of the horizontal scattering arms is related inversely to the aspect ratio of the fiber, with high-aspect ratio fibers producing the thinnest scattering. In both chrysotile and crocidolite fibers, the fiber volume may be related to a first approximation to the total scattered light recorded.

The particle scattering profile examples given in Fig. 3 illustrate some of the morphology-dependent features whose recognition and analysis may offer a potential route to particle classification. In addition, the figure offers the prospect of identifying asbestoslike fibers from background airborne particulates and of possibly discriminating between chrysotile fibers and crocidolite (and similar fiber types). Below we describe an instrument that seeks to exploit this opportunity.

2. Determination of Optimal Detector Geometry

We determined the optimal design for the detector array to be used in the new instrument by simulating the performance of a variety of possible configurations and assessing their performance in terms of particle discrimination efficiency and processing speed for a variety of different processing algorithms.

We achieved the computer simulation by mapping each possible detector design onto each of several thousand scattering profiles (similar to those shown in Fig. 3) for various particle types recorded using the intensified camera system described above. Detector designs varied from a simple 8-element radial array to a 64-element array configured in nonuniform offset rings. For each element of an array, the simulated scattered light signal was determined by integration over the corresponding area of the scattering profile image. The simulated detector outputs for each detector array geometry were then passed for analysis to each of four commonly used data classification methods: normal distribution, linear discriminant, k-nearest neighbors, and radial basis function (RBF) neural network. (The detailed operation of these classification algorithms is not given here, and the interested reader is directed to one of the many excellent texts on classification theory, for example, *Pattern Classification and Scene Analysis*,¹⁰ for more information.) Each of the classification methods required the presence of class templates against which the incoming particle data could be compared and subsequently classified. These templates were computed for each detector geometry

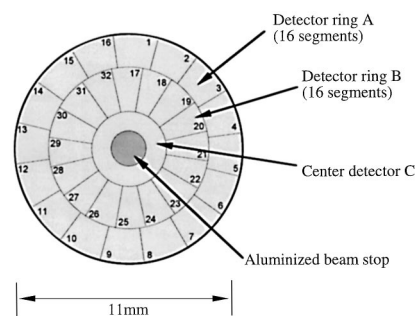


Fig. 4. Outline diagram of the layout of the custom multielement photodiode detector array used in the new instrument to collect light scattered from individual particles. The array is 11 mm in diameter and is configured on a single silicon substrate. The numbers that appear in each detector element are given to aid comparison with the examples of actual light scattering data given in Fig. 9.

from a base of typically 100 images from each of chrysotile fiber scattering profiles, crocidolite profiles, and randomly selected profiles recorded from background airborne particulates (see Section 4). As many as ten thousand scattering profile images recorded from known aerosols of each particle type were subsequently analyzed by each of the four classification methods and for each of the detector array geometries. This allowed the determination of the specific combination of detector geometry and classification method that yielded optimal particle classification accuracy and speed of execution within the constraints of conventional personal computer processing performance.

The outcome of this simulation exercise established that the detector geometry shown in Fig. 4, in combination with the RBF neural network classification method, gave optimal particle classification performance. The 33-element detector array comprised two annular rings, labeled A and B in Fig. 4, each divided into 16 detector elements. These surrounded a center annular ring, labeled C, which could be used in conjunction with the other detector elements to estimate a spherical equivalent particle size (from Mie theory¹¹). The concentric ring detectors A and B provide the spatial scattering data required for particle classification. The ring offset was to minimize the possibility of fine fiber scattering from elongated fibers lying entirely along the dead zones between adjacent detector elements in both the A and the B segmented rings.

The RBF network is arguably one of the simplest forms of an artificial neural network. It is based on the use of training data, in our case these being example sets of 100 scattering patterns from each of the particle classes that we wish to discriminate. The training data result in defined regions of mathematical hyperspace corresponding to the chosen classes. When new data (expressed as an input vector) derived from an unknown particle are input to the network, the network evaluates the distance between this input vector and its predefined class data regions

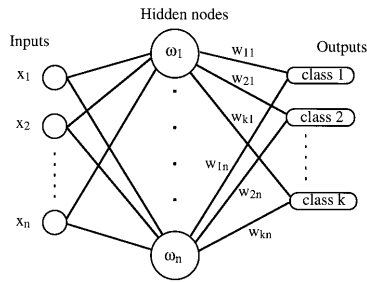


Fig. 5. Schematic illustration of the basic elements of a RBF neural network.

and indicates to which class the unknown particle corresponds most closely.

The RBF network has an architecture consisting of only one hidden layer, as illustrated in Fig. 5. In our case, the inputs, labeled x_1 to x_n were the values of the light-scattering data from either the A or B detector ring; these were processed independently through the network so as to allow a voting on the classification outcome. Only if both processes resulted in the same classification for a particle (judged as that having the highest linear summation output value) was the particle ascribed to that class (shown as class 1, class 2, etc., in Fig. 5). If there was a discrepancy in classification results from the two detector rings, the particle was classified into the lower of the two classes.

The hidden nodes ω_1 to ω_n are RBF's that take the form

$$\omega_i(\|x - x_i\|), \quad (1)$$

where $\omega_i(\bullet)$ is a nonlinear function of the distance between the input vector x (based on the detector ring values for the unknown particle) and the i th center vector x_i (marking the hyperspace region corresponding to each prescribed class of particle). The network output vector class is simply the linear summation of the weighted basis functions

$$\text{class}_j = \sum_{i=1}^n w_{ji} \omega_i(\|x - x_i\|), \quad j = 1, 2, \dots, k, \quad (2)$$

the weights for each class $w_{11}, w_{21}, \dots, w_{kn}$ having been established by the training data. In our case, the RBF's were chosen to be Gaussian, a commonly used approach and one that gave good classification results. The functions were of the form

$$\omega_i(\|x - x_i\|) = \exp\left(-\frac{\|x - x_i\|^2}{d^2}\right), \quad (3)$$

where d is a constant bandwidth parameter.

Figure 6 summarizes the simulated classification performance of the selected detector geometry and the RBF analysis method. Some 10,000 examples of scattering profiles recorded from known aerosols of each of the three chosen particle types (chrysotile, crocidolite, and background) were processed and clas-

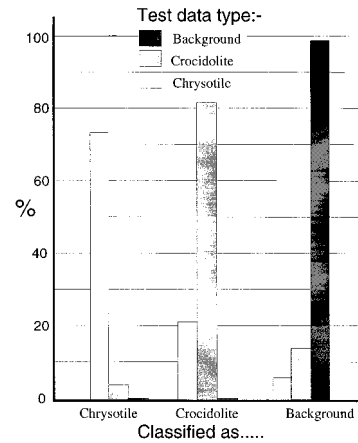


Fig. 6. Graphical representation of the simulated performance of the detector configuration (shown in Fig. 4) and the RBF neural network in terms of classifying particles from known aerosols. Ideally, 100% of each test data type should be classified into its correct class.

sified into their respective classes. Ideally, 100% of each input test data type should be classified into its correct particle class. In practice, over 99% of background particles were classified correctly as background, with 0.1% being misclassified as chrysotile particles and 0.6% misclassified as crocidolite. These misclassification figures are a result of nonasbestos fibers within the background sample producing scattering profiles sufficiently similar to the extremes of the chrysotile or crocidolite classes that they were classified as such. They therefore represent a threshold level against which actual fiber concentration measurements must be compared. Similarly, over 80% of crocidolite and 70% of chrysotile particles were classified correctly. The misclassification of the remainder of these particles into the background class is inevitable when this laser scattering technique is used because some crocidolite or chrysotile particles are aerosolized as irregular clumps or fiber aggregates that do not produce characteristic fiber scattering. The consequence will be the underestimation of the true asbestos fiber concentration by some small margin, although this parallels the decision processes that occur during the standard phase contrast light microscope filter sample counting technique (see Section 4).

3. Instrumentation

The new fiber characterization instrument incorporates the selected detector geometry as a custom photodiode array chip, manufactured by Centronic, Ltd., Croydon, England. The chip has a diameter of 11 mm and is mounted into a commercial pin grid-array package with no covering window. The complete instrument is shown schematically in Fig. 7. The laser scattering chamber is similar in principle to that used with the intensified CCD camera system (Fig. 2), with the exception that the low-power diode laser has been replaced with a high-power 100-mW, 670-nm wavelength diode laser (Power Technology,

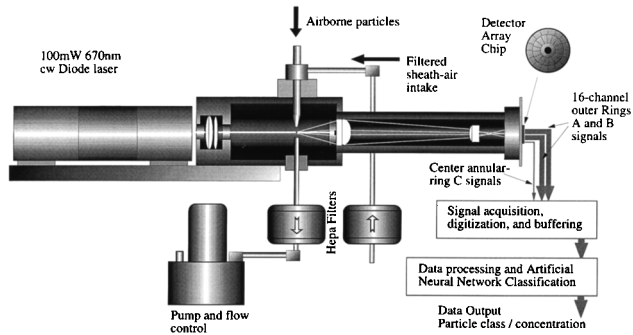


Fig. 7. Schematic diagram of the new laser scattering instrument that incorporates the custom photodiode detector array to collect light scattered from individual particles carried in the sample airstream.

Inc., Little Rock, Arkansas) to compensate for the fact that the photodiode array has no inherent gain and would be incapable of providing adequate output signals if used with the low-power laser. (Again, the laser output is linearly polarized in the plane of the diagram.) The beam cross section at the intersection with the sample airflow is of ellipsoidal shape, approximately 2 mm in width and 120 μm in depth, leading to a particle transit time through the beam of $\sim 5 \mu\text{s}$. Sample airflow through the device is set to be 1 l/min. Because particle trajectories through the beam could take place anywhere within the horizontal cross-sectional area of the sample air column (approximately 1 mm in diameter), the scattered light capture optics were designed to ensure that such particle trajectory variation did not cause significant translation of the scattering profile image on the detector array. The center detector ring C receives light scattered between 4° and 10° to the primary beam axis; the second and third rings, B and A, receive light scattered between 10° and 18° and 18° and 28° , respectively.

The operation of the signal acquisition, digitization, and buffering electronics is shown schematically in Fig. 8. When a particle enters the laser beam the signal received from the central annular ring C begins to rise. This rise is detected by a particle trigger detection circuit that initiates data acquisition from the other 32 detector elements. This acquisition is achieved by two dedicated application-specific integrated circuit chips, labeled HX2 in Fig. 8. These chips are manufactured by Rutherford Appleton Laboratories, Didcot, U.K. Each HX2 chip contains 16 parallel integrators that integrate the signals from the individual detector elements for the duration of the particle transit through the beam. The chips then hold these analog signal values and serially multiplex them out to analog-to-digital converters. FIFO (first in first out) buffers subsequently store the digital data, 33 values per particle, before transferring them at an optimal rate to the neural network data processing system (based on dual Motorola 68040 processors) for particle classification.

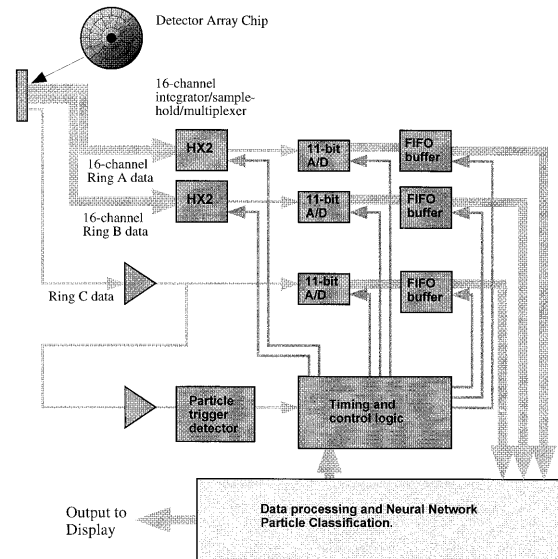


Fig. 8. Schematic diagram showing the acquisition and digitization process for light-scattering signals derived from the custom detector array chip.

Figure 9 shows typical examples of the type of detector data fed to the neural network for analysis and pattern classification. The examples show typical scattering data recorded from a crocidolite fiber, a chrysotile fiber (both derived from the Union International de la recherche Contre le Cancer reference materials referred to above), and an irregular-shaped background particle. Examples similar to these constituted the class-template data used to train the neural network. Data elements labeled 1–16 represent the output from the outer detector ring A, and those labeled 17–32 represent the output from the middle ring B; as a consequence, crocidolite fiber scattering produces four sharp peaks, chrysotile produces four broad peaks, and the background particle produces an irregular pattern. The data have been normalized to the highest data element in each case. Note that the output from the 33rd element, the center ring C, which is used to provide an approximate assessment of particle size, is not shown in Fig. 9. The output from this detector element does not normally form part of the neural network analysis since to do so could create the possibility of the particle classifications being unduly biased on the basis of particle size rather than shape (or, more correctly, scattering asymmetry).

To assess the performance of the machine neural network against results achieved by manual classification, we carried out experiments using aerosols containing mixed particle types. For each aerosol, data relating to 3000 particles were classified, first by visual inspection by a trained volunteer and second by use of the RBF neural network classifier. The data were of the form similar to that shown in Fig. 9. Because these mixed aerosols contained crocidolite, chrysotile, and background particles and it was known that some overlap in the scattering character-

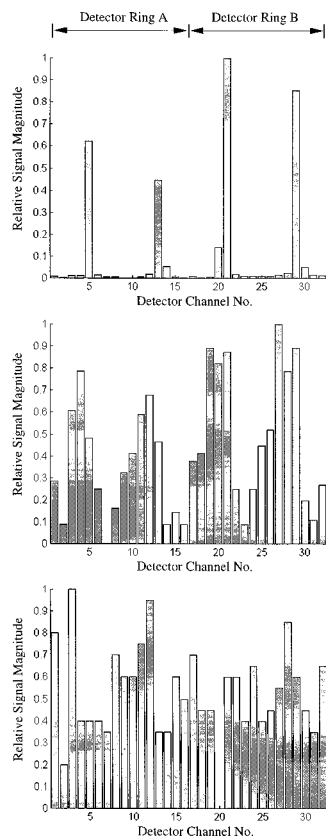


Fig. 9. Typical examples of the output of the detector system of the new instrument. These show the scattered light intensities received by each of the 32 detector channels (1–16 from the outer detector ring A and 17–32 from the middle ring B; refer to Fig. 4) for a single crocidolite asbestos fiber (top), a single chrysotile fiber (middle), and an irregular background particle. Data of this format are fed to the neural network for pattern classification.

istics of these materials was inevitable (as illustrated in Fig. 6), the classifications used were high-risk fibers (those that displayed predominantly crocidolite-like scattering features), medium-risk fibers (those that displayed predominantly chrysotilelike scattering features), and other particles. Table 1 summarizes the results for one such mixed aerosol, illustrating the close similarity in classification performance between machine and manual classifica-

Table 1. Summary of the Classification of Scattering Profile Data from a Mixed Aerosol Containing Crocidolite, Chrysotile, and Background Particles^a

Particle Class	Manual Classification (%)	RBF Neural Network Classification (%)
High-risk fibers	4.4	4.3
Medium-risk fibers	15.4	14.3
Other particles	80.2	81.4

^aThe classification was achieved both by visual inspection of graphical data (similar to those shown in Fig. 9) and by RBF neural network analysis. High-risk fibers are those that display crocidolite-like scattering profiles; medium-risk fibers are those that display chrysotilelike scattering.

tions—the significant difference being that the manual classification required several hours (similar to that required for phase contrast light microscope fiber counting on filters), whereas the machine classification required only seconds.

4. Discussion

The established method of fiber contamination assessment with filter sampling followed by phase contrast microscopy is known to have disadvantages in terms of the prolonged analysis time required and the inevitable subjectivity in the counting introduced by each individual microscopist. Nevertheless, it remains the standard method by which all other methods will be judged. Despite its near real-time response, the light-scattering method that we described in this paper would gain acceptance only if the results it gave were close to those that the standard method would have given under similar measurement conditions. The authors are therefore currently undertaking a series of field experiments in actual asbestos clearance operations during which measurements are taken using both the standard filter method and the light-scattering technique to allow such comparisons to be made. Here the use of a neural network provides a useful means for the output of the classification process to be tuned so as to bring it into line with that of a microscopist that uses the filter analysis. With phase contrast imaging microscopy of filter samples there exists a continuum of possible fiber presentations (crossed fibers, multiple fibers, fibers attached to other particles, etc.) about which the microscopist must make a decision. Similarly, in the case of the light-scattering data presented to the neural network, there exists a continuum of scattering patterns (similarly due to single fibers, multiple fibers, fibers attached to other particles, etc.) about which the neural network computes a decision based on its training template data. For example, a microscopist may exclude a fiber because it has attached to it a comparatively large non-fibrous particle; similarly, the neural network would reject the scattering pattern from such a composite particle because of the severe perturbation from ideal fiber scattering that the subparticle would cause. Thus, by appropriate selection of the training template data, the breadth of light-scattering patterns that the neural network regards as, say, hazardous fibers, may be adjusted so as to be in accord with that produced by the trained microscopist assessing fiber images on a filter substrate. If this process is successfully achieved, the light-scattering method could provide a valuable real-time alternative to filter sampling fiber contamination assessment.

This research has been supported by grants from the U.K. Engineering and Physical Sciences Research Council and Department of Trade and Industry. The asbestos fiber aerosol measurements were made at the Medical Research Council's Toxicology Laboratories, Leicester, U.K., under the direction of J. A. Hoskins.

References and Notes

1. R. C. Brown, J. A. Hoskins, and N. F. Johnson, eds., *Mechanisms in Fiber Carcinogenesis*, *Life Science*, Vol. 223 (Plenum, New York, 1991), pp. 1–589.
2. J. Peto, J. T. Hodgson, F. E. Matthews, and J. R. Jones, “Continuing increase in mesothelioma mortality in Britain,” *Lancet* **345**, 535–539 (1995).
3. Testimony of NIOSH on occupational exposure to asbestos, tremolite, anthrophyllite, and actinolite. 29CFR, Parts 1910 and 1926, 9 May 1990.
4. J. Carter, D. Taylor, and P. A. Baron, “Fibers method 7400 revision no. 3:5/15/89” in *NIOSH Manual of Analytic Methods* (U.S. Department of Health and Human Services, Washington, D.C., 1989).
5. P. Lilienfeld, P. Elterman, and P. Baron, “Development of a prototype fibrous aerosol monitor,” *Am. Ind. Hyg. Assoc. J.* **40**, (4), 270–282 (1979).
6. P. A. Baron, M. K. Mazumder, and Y. S. Cheng, “Direct reading techniques using optical particle detection,” in *Aerosol Measurement*, K. Willeke and P. A. Baron, eds. (Reinhold, New York, 1993), pp. 403–408.
7. A. P. Rood, E. J. Walker, and D. Moore, “Construction of a portable fibre monitor measuring the differential light scattering from aligned fibres,” in *Proceedings of the International Symposium: Clean Air at Work*, R. H. Brown, M. Curtis, K. J. Saunders, and S. Vandrendreissche, eds. (Royal Society of Chemistry, London, 1992), pp. 265–267.
8. E. Hirst, P. H. Kaye, and J. Guppy, “Light scattering from non-spherical airborne particles: experimental and theoretical comparisons,” *Appl. Opt.* **33**, 7180–7186 (1994).
9. P. H. Kaye, K. Alexander-Buckley, E. Hirst, and S. Saunders “A real-time monitoring system for airborne particle shape and size analysis,” *J. Geophys. Res.* **101**, 19,215–19,221 (1996).
10. R. O. Duda and P. E. Hart, *Pattern Classification and Scene Analysis* (Wiley, New York, 1973).
11. C. F. Bohren and D. R. Huffman, *Absorption and Scattering of Light by Small Particles* (Wiley, New York, 1983).